Small-Signal Analysis of Amplitude-, Phase-, and Polarization-to-Intensity Conversion in General Optical Linear Systems With Application to PMD Compensation

Alberto Bononi and Alessandra Orlandini, *Member, IEEE*

***Abstract*—A general small-signal model for amplitude-, phase-, and polarization-to-intensity conversion in optical systems affected by chromatic dispersion, polarization-mode dispersion (PMD), and polarization-dependent loss (PDL) is presented, which extends a previous scalar model by Wang and Petermann [1]. The model leads to simple intensity filters, which can be expressed as a linear combination of the components of the Stokes' vector of the signal input state of polarization (ISOP), and facilitates the prediction of the ISOPs, which minimize/maximize the intensity modulation on the output signal. The model is first used to study the output intensity in a first-order PMD-compensated single-channel system with either input amplitude, or phase, or polarization modulation. The small-signal model provides a good prediction of the received intensity up to modulation indexes of about 20%–30%, according to the modulation type. The model is then successfully used in a semianalytical bit-error rate (BER) evaluation method to estimate the system penalty induced by cross-phase modulation (XPM) in a two-channel wavelength-division-multiplexed (WDM) dispersion-managed system with PMD compensation.**

***Index Terms*—Nonlinearity, optical fibers, polarization, polarization-mode dispersion (PMD), polarization-mode dispersion (PMD) compensation.**

I. Introduction

IT has recently been shown that the performance of wavelength-division-multiplexed (WDM) systems with optical polarization-mode dispersion compensators (OPMDCs) can be severely degraded by cross-phase modulation (XPM)-induced depolarization [2]–[4]. Such compensators, usually designed for the single-channel linear propagation regime, are based on a small-bandwidth feedback control and are thus not able to follow the bit-by-bit XPM distorting effects. Moreover, the presence of residual chromatic dispersion (CD) and/or lumped polarization-dependent loss (PDL) causes additional distortions that interact with those due to the polarization-mode dispersion (PMD)/XPM interaction [5], further degrading the OPMDC efficiency.

Although some simple, convincing arguments have been provided in [3] to explain the degradation mechanism due to the interplay of XPM and PMD in OPMDCs with ON–OFF keying (OOK) modulation, a complete system model for the quantification of such a degradation, mainly due to the distributed conversion of XPM-induced polarization modulation to intensity modulation along the fiber, is still not available.

Following in the footsteps of the development of a successful distributed *scalar* model for the evaluation of the amplitude- and phase-to-intensity modulation (AM–IM, PM–IM) conversion in dispersion-managed optical fiber systems affected by both XPM and chromatic dispersion [6]–[8], which capitalized on the results of the Wang–Petermann small-signal IM–IM, PM–IM *scalar* model [1], this paper presents the key result needed for the extension of the model in [6] to the case of optical systems also affected by PMD and PDL, namely, a *vectorial* version of the Wang–Petermann small-signal model. While the IM–IM *vectorial* case was already tackled by Noé *et al.* [9] for systems without PDL, and a large-signal IM–IM analysis was introduced in [10] for systems without PDL and in [11] for systems with PDL, the new contribution of this paper is the study of the small-signal *vectorial* model of both common-mode PM–IM and polarization modulation to intensity modulation (PolM–IM), which are needed tools to cope with phase and polarization modulations induced by XPM in WDM systems.

While previous analyses have dealt with input polarization modulation by considering an equivalent relative motion of the fiber principal states of polarization (PSP) with respect to a fixed input state of polarization (ISOP) [12], [2], an approach that is correct only when the bandwidth of the polarization-modulated signal is much smaller than the PSP's bandwidth (a quasi-static approach), a valuable element of novelty of this paper is the rigorous analytical treatment of fast (bit-by-bit) input polarization modulation, which is needed when the signal bandwidth exceeds that of the PSP's and significant higher order PMD is present.

The paper is organized as follows. In Section II, the generalized vectorial small-signal model is introduced, providing a very compact expression of the AM–IM, PM–IM, and PolM–IM filters expressed as linear combinations of the four-dimensional Stokes' vector of the unperturbed ISOP. Section III presents an application of the previously generalized model to linear fiber systems affected by CD, PDL, and all-order PMD, both with and without first-order OPMDC. Typical functional shapes of the AM–IM, PM–IM, and PolM–IM filters versus frequency are presented, and the accuracy of the small-signal model is checked against direct simulation. Section IV shows the use of

Manuscript received October 20, 2003; revised September 30, 2004. This work was developed within the framework of a collaboration between the University of Parma and Alcatel Research and Innovation, Marcoussis, France.

The authors are with the Dipartimento di Ingegneria dell'Informazione, Università di Parma, 43100 Parma, Italy (e-mail: bononi@tlc.unipr.it).

Digital Object Identifier 10.1109/JLT.2004.839976

the model in a semianalytical bit-error rate (BER) evaluation tool for system penalties assessment in WDM dispersion-managed systems affected by XPM and PMD. Finally, findings are summarized in Section V.

II. Generalized Small-Signal Model

Consider a general linear optical transmission system, described by a 2×2 Jones matrix $T(\omega)$, which accounts for CD, PMD, and PDL. Assume the 2×1 complex envelope of the input field is composed of a continuous-wave (CW) component plus a *small* perturbation as $\mathbf{E}_i(t)=E_i(1+a(t))e^{-i\theta_c(t)}\mathbf{J}(t)$, where E_i is a constant scalar amplitude, $a(t)$ a *small* real amplitude modulation, and $\theta_c(t)$ a *small* real common-mode phase modulation, and the ISOP vector $\mathbf{J}(t)$ is also modulated. Since the polarization modulation operated by XPM shows up in the Stokes' space as a time rotation of the state of polarization (SOP) around a given axis [5], [3], [4], we will assume that the ISOP takes the form $\mathbf{J}(t)=U_p(t)\mathbf{J}_i$, where the unitary time-varying operator associated with the Jones matrix $U_p(t)$ operates a counterclockwise rotation of the unit Stokes' 3×1 vector $\widehat{j}$ associated with the Jones vector $\mathbf{J}_i$ around a fixed Stokes' unit axis $\hat{p}$ by a time-varying *small* polarization modulation angle $2\theta_p(t)$. Analytically, the Jones matrix of this rotation operator takes the form $U_p=\cos(\theta_p)\sigma_0-i\sin(\theta_p)(\hat{p}\cdot\vec{\sigma})$, where σ_0 is the 2×2 identity matrix, $\vec{\sigma}=[\sigma_1;\sigma_2;\sigma_3]$ the 3×1 Pauli spin vector whose elements are the 2×2 Pauli matrices σ_i, and the symbol $\cdot$ denotes the scalar (inner) product so that $\hat{p}\cdot\vec{\sigma}=\sum_{i=1}^{3}p_i\sigma_i$ is a 2×2 matrix [13], [10]. A good summary on the use of Pauli matrices in PMD-related problems can be found in [13]. Being the modulations $a(t)$, $\theta_c(t)$, and $\theta_p(t)$ much smaller than one, one can approximate the input field as $\mathbf{E}_i(t)\cong E_i[\mathbf{J}_i+\Delta\mathbf{J}_i(t)]$, where $\Delta\mathbf{J}_i(t)=[(a(t)-i\theta_c(t))\mathbf{J}_i-i\theta_p(t)\mathbf{L}]$ and $\mathbf{L}\triangleq(\hat{p}\cdot\vec{\sigma})\mathbf{J}_i$. The Fourier transform of the output field is $\mathbf{E}_o(\omega)=T(\omega)\mathbf{E}_i(\omega)=E_i[\mathbf{J}\delta(\omega)+\Delta\mathbf{J}(\omega)]$, where $\mathbf{J}\triangleq T(0)\mathbf{J}_i$, $\delta(\omega)$ is the Dirac delta, and $\Delta\mathbf{J}(\omega)\triangleq T(\omega)\Delta\mathbf{J}_i(\omega)$. Consequently, the time-domain output intensity $I(t)=|\mathbf{E}_o(t)|^2$ can be expressed as

$$I(t)=\langle I\rangle(|\mathbf{J}|^2+2\Re[\mathbf{J}^\dagger\Delta\mathbf{J}(t)]+|\Delta\mathbf{J}(t)|^2) \tag{1}$$

where $\langle I\rangle=|E_i|^2$ is the input CW intensity, the $\dagger$ denotes the transpose conjugation, $\Re[x]$ denotes the real part of x, and the term $\Delta\mathbf{J}(t)$ is the inverse Fourier transform of $\Delta\mathbf{J}(\omega)$. After dropping the *small* $|\Delta\mathbf{J}|^2$ term, one can finally express the small-signal output intensity perturbation on the CW $\Delta I\triangleq I-\langle I\rangle|\mathbf{J}|^2$ in the frequency domain as

$$\Delta I(\omega)=\langle I\rangle[H_a(\omega)a(\omega)+H_c(\omega)\theta_c(\omega)+H_p(\omega)\theta_p(\omega)] \tag{2}$$

where $a(\omega)$, $\theta_c(\omega)$, and $\theta_p(\omega)$ are the Fourier transforms of the real modulations $a(t)$, $\theta_c(t)$, and $\theta_p(t)$, respectively, and

$$\begin{aligned}H_a(\omega)&=\mathbf{J}_i^\dagger[V(\omega)+V^\dagger(-\omega)]\mathbf{J}_i\\ H_c(\omega)&=\mathbf{J}_i^\dagger[V(\omega)-V^\dagger(-\omega)]\mathbf{J}_i/i\\ H_p(\omega)&=[\mathbf{J}_i^\dagger V(\omega)\mathbf{L}-\mathbf{L}^\dagger V^\dagger(-\omega)\mathbf{J}_i]/i\end{aligned} \tag{3}$$

are the AM–IM, common-mode PM–IM, and PolM–IM small-signal frequency responses, respectively, and $V(\omega)\triangleq T^\dagger(0)T(\omega)$. Note that the first of such relationships[1] was already implicitly used in [9] for the analysis of the feedback signal in PMD compensators. The remaining two filters in (3) are original results of this paper. Such filters are already in an analytical form suitable for numerical analysis. However, it is possible to recast them in a form that allows a geometrical interpretation of their dependence on the unperturbed ISOP.

To this aim, we decompose the Jones matrix $V(\omega)$ on the basis of Pauli matrices as $V(\omega)=\sum_{i=0}^{3}v_i(\omega)\sigma_i=\underline{v}(\omega)\cdot\underline{\sigma}$, with $\underline{v}(\omega)=[v_1;v_2;v_3;v_4]$ being its 4×1 vector of Pauli coordinates (which we call the *Pauli vector*) and $\underline{\sigma}\triangleq[\sigma_0;\vec{\sigma}]$ [10]. Now, plug such an expression of $V(\omega)$ in (3), and then use standard manipulation rules for Pauli spin vectors [13], [14]. The end result, which is derived in Appendix A, can be compactly expressed by introducing the following definitions.

Let $\underline{j}=[1;\hat{j}]$ be the 4×1 Stokes' vector associated with $\mathbf{J}_i$ (i.e., $\underline{j}=\mathbf{J}_i^\dagger\underline{\sigma}\mathbf{J}_i$), and define the 4×4 block-partitioned matrix

$$P\triangleq\begin{bmatrix}0 & \hat{p}^T\\ \hat{p} & i\hat{p}\times\end{bmatrix}$$

where $\hat{p}\times$ is the cross-product 3×3 matrix generated by the 3×1 unit vector $\hat{p}$ [13, eq. (4.8)], and the symbol ^{T} denotes transposition. Now, define $\underline{v}_R(\omega)\triangleq(\underline{v}(\omega)+\underline{v}^*(-\omega))/(2)$ and $\underline{v}_I(\omega)\triangleq(\underline{v}(\omega)-\underline{v}^*(-\omega))/(2i)$, where * denotes conjugation. Finally, define $\underline{z}(\omega)\triangleq P^T\underline{v}(\omega)$ and $\underline{z}_I(\omega)\triangleq(\underline{z}(\omega)-\underline{z}^*(-\omega)/2i)$. Then, the frequency responses (3) can be compactly rewritten as

$$\begin{cases}H_a(\omega)=2\underline{v}_R(\omega)\cdot\underline{j}\\ H_c(\omega)=2\underline{v}_I(\omega)\cdot\underline{j}\\ H_p(\omega)=2\underline{z}_I(\omega)\cdot\underline{j}\end{cases} \tag{4}$$

which represent the main theoretical contribution of this paper. From such relations, it is clear that the frequency responses are a linear combination of the four entries of the unperturbed ISOP Stokes' vector. Therefore, it is now simple to find the "best" and "worst" ISOPs of the system [11]. For instance, the IM–IM small-signal frequency response was shown in [10, eq. (55)] to be $H_{\mathrm{IM}}(\omega)=\underline{v}_R(\omega)\cdot\underline{j}$, that is, half the AM–IM response $H_a(\omega)$, and the magnitude of $H_{\mathrm{IM}}(\omega)$ at $\omega_0=2\pi(R/2)$ (with R being the signal bit rate) was shown to be a good estimate of the eye opening at small eye-closure penalty (ECP) values [10, eq. (50)]. In addition, it was shown that the best/worst ISOPs $\underline{j}$ for the IM response in an uncompensated system obtained from the small-signal model do coincide with the best/worst ISOPs of the exact large-signal model [10, Figs. 12 and 13].

In the following, we will show how the PM–IM filter H_c and the PolM–IM filter H_p can be applied to the description of scalar and vectorial XPM effects in WDM systems with PMD [4] and can thus be usefully exploited in the assessment of system penalties.

[1]More precisely, the IM–IM filter, which differs from the AM–IM filter by a factor of 2.

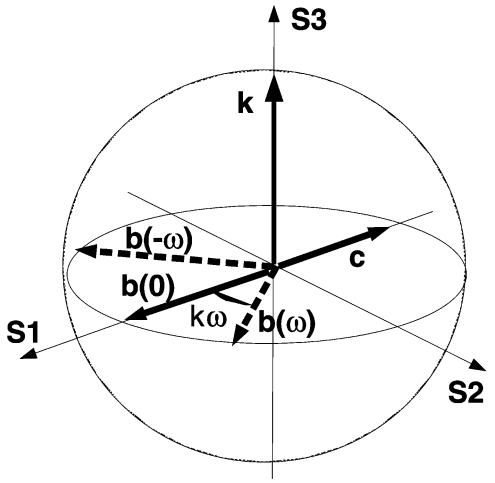

Fig. 1. Line and compensator eigenmodes and eigenmodes rotation axis on the Poincaré sphere.

III. Application to First-Order PMD-Compensated Systems

We now show the usefulness of relations (4) when analyzing the intensity modulation induced by (desired) amplitude modulation and (often accidental) phase and polarization modulation, such as those induced by XPM, at the output of a system composed of a linear transmission line followed by a first-order OPMDC.

First, assume the fiber line has no PDL, and a unitary Jones matrix $U_F(\omega) = V_L(\omega)U_{F0}$, where U_{F0} is its value at the reference frequency, and $V_L(\omega)$ is the unitary extracted Jones matrix (also known as difference rotation matrix [15]), which we model as $V_L(\omega) = \cos(\Delta\tau\omega/2)\sigma_0 - i\sin(\Delta\tau\omega/2)(\hat{b}(\omega)\cdot\vec{\sigma})$, where $\Delta\tau$ is the differential group delay (DGD), and $\hat{b}(\omega)$ is the unit eigenmode, which at the carrier frequency ($\omega = 0$) is aligned with the line input PSP [10, eq. (30)]. This form of the line Jones matrix implies a general depolarizing trajectory of the eigenmode $\hat{b}(\omega)$, or equivalently of the PSP, and assumes that the DGD does not vary with frequency, that is, neglects polarization-dependent chromatic dispersion, which is known to contribute way less severely than the eigenmodes (PSP) depolarization to system degradation [16]. For simplicity, we will assume that the eigenmode $\hat{b}$ follows a *rotation model* [10, p. 268], that is, rotates, as ω varies, at a constant rotation speed k around a fixed (unit) rotation axis $\hat{k}$ coinciding with the vertical Stokes' axis $\hat{s}_3$, starting from $\hat{b}(0)$ coinciding with the first Stokes' axis $\hat{s}_1$, which represents a worst case for the eigenmodes depolarization (equatorial trajectory).

We assume the line is followed by a single-stage OPMDC, based on a polarization maintaining fiber of DGD exactly $\Delta\tau$, whose PSP direction vector $\hat{c}$ is placed so as to cancel the first-order PMD of the line, that is, it is aligned with $-\hat{b}(0)$. Such a scheme implements an ideal first-order compensation, which completely equalizes the line in the absence of depolarization (higher order PMD), that is, when $\hat{b}(\omega) \equiv \hat{b}(0)$. The positions of the line and compensator eigenmodes on the Poincaré sphere are depicted in Fig. 1.

One can show (Appendix B) that in the absence of line CD, the overall line + OPMDC system has a Jones matrix whose Pauli coordinates yield

$$\underline{v}_R(\omega) = \left[\cos^2\left(\frac{\Delta\tau\omega}{2}\right) + \sin^2\left(\frac{\Delta\tau\omega}{2}\right)\cos(k\omega);\right.$$
$$\left. i\sin(\Delta\tau\omega)\sin^2\left(\frac{k\omega}{2}\right); 0; i\sin^2\left(\frac{\Delta\tau\omega}{2}\right)\sin(k\omega)\right]$$
$$\underline{v}_I(\omega) = \left[0; 0; -\frac{1}{2}\sin(\Delta\tau\omega)\sin(k\omega); 0\right]$$

so that one explicitly finds

$$\begin{aligned}
H_a(\omega) &= 2\left[\cos^2\left(\frac{\Delta\tau\omega}{2}\right) + \sin^2\left(\frac{\Delta\tau\omega}{2}\right)\cos(k\omega)\right] \\
&\quad + 2i\left[\sin^2\left(\frac{\Delta\tau\omega}{2}\right)\sin(k\omega)j_3\right. \\
&\quad \left. + \sin(\Delta\tau\omega)\sin^2\left(\frac{k\omega}{2}\right)j_1\right] \\
H_c(\omega) &= -\sin(\Delta\tau\omega)\sin(k\omega)j_2 \\
H_p(\omega) &= -\sin(\Delta\tau\omega)\sin(k\omega)p_2 \\
&\quad + 2i\left[\sin^2\left(\frac{\Delta\tau\omega}{2}\right)\sin(k\omega)(p_1j_2 - p_2j_1)\right. \\
&\quad \left. + \sin(\Delta\tau\omega)\sin^2\left(\frac{k\omega}{2}\right)(p_2j_3 - p_3j_2)\right] \quad (5)
\end{aligned}$$

where $\hat{j} = [j_1; j_2; j_3]$ and $\hat{p} = [p_1; p_2; p_3]$.[2] From (5), we note that the AM–IM filter does not depend on the unperturbed ISOP component j_2, while the PM–IM conversion only depends on such an ISOP component. Consequently, the worst ISOPs in the AM case are $\hat{j} = \pm\hat{s}_2$, since the magnitude $|H_a(\omega)|$ is minimum for all frequencies. In addition, no PM–IM conversion takes place for those ISOPs lying on the plane $(\hat{s}_1, \hat{s}_3)$ containing $\hat{b}(0)$ and the eigenmode rotation axis $\hat{k}$, while maximum PM–IM conversion occurs for $\hat{j} = \pm\hat{s}_2$, that is, the ISOPs perpendicular to such a plane. Note also from (5) that the real part of the PolM–IM filter is functionally a multiple of the PM–IM filter, while its imaginary part vanishes when $\hat{j}$ is aligned with the rotation axis $\hat{p}$.[3] Hence, polarization modulation gives a much smaller intensity distortion than common-mode phase modulation ($|H_p(\omega)| < |H_c(\omega)|$) when $p_2 \ll j_2$ and $\hat{j}$ is almost aligned with $\hat{p}$. Note that the presence of CD and PDL considerably complicates the expressions of the previously described filters.

We now provide numerical verifications of these filters in order to clarify the usefulness of the previously provided formulas. In the calculations, the input CW had unit intensity $E_i = 1$, and the line had DGD $\Delta\tau = 0.5T$ and eigenmode depolarization rate $k = 0.2T$, with T being the bit time of a digitally modulated signal of interest. The unperturbed ISOP $\hat{j}$ had azimuth $\theta = \pi/4$ and ellipticity $\varepsilon = \pi/12$, with equal power split on the PSPs.

[2]The Stokes' vectors $\hat{j}$ and $\hat{p}$ we use here correspond to those rotated by the operator U_{F0}, as explained in Appendix B.

[3]We note here that, for the chosen structure of $U_p(t)$, the largest input depolarization is obtained when $\hat{p}$ is orthogonal to $\hat{j}$, while when $\hat{p}$ is aligned with $\hat{j}$, one gets $\mathbf{L} \equiv \mathbf{J}_i$ and thus $H_p(\omega) \equiv H_c(\omega)$, as one can also deduce directly from (4).

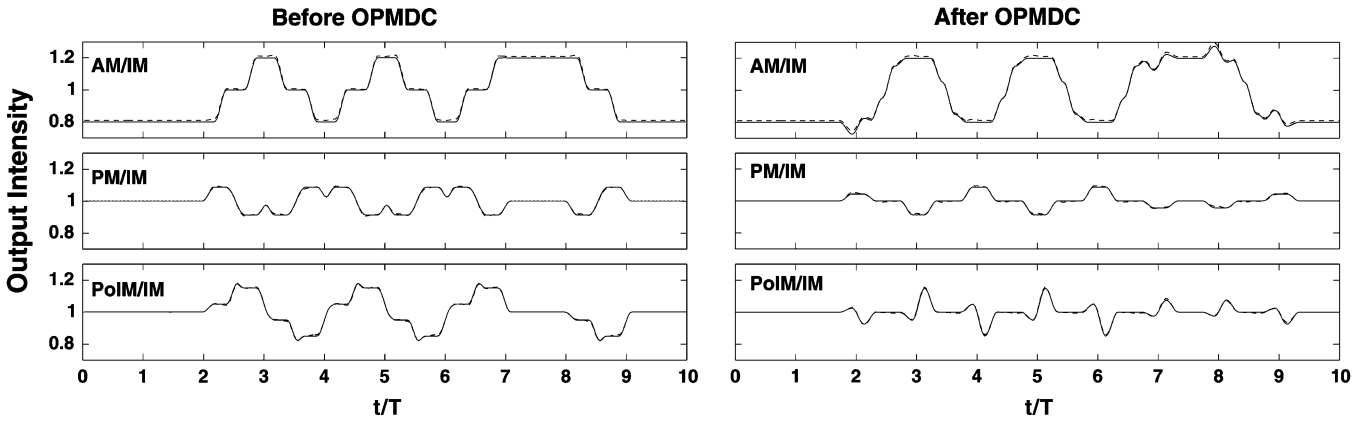

Fig. 2. Output intensity before (left) and after (right) the OPMDC when either AM (top), PM (center), and PolM (bottom) are applied, with a 10% modulation index and $E_i = 1$. Line parameters: $\Delta\tau = 0.5T$, $k = 0.2T$. Unperturbed ISOP: azimuth $\theta = \pi/4$, ellipticity $\varepsilon = \pi/12$. Solid line: Small-signal model. Dashed line: Exact solution.

Fig. 2 shows the output intensity before (left column) and after (right column) the OPMDC, when modulation of *either* the amplitude a (top), *or* the common phase θ_c (center), *or* the polarization angle θ_p (bottom) was introduced by the bit sequence 0 001 010 110 of nonreturn-to-zero (NRZ) pulses swinging from -0.1 to 0.1, yielding a modulation index of 10% in all three cases. The pulse shape was a raised cosine, with roll-off 0.2. The polarization modulation axis $\hat{p}$ was orthogonal to $\hat{j}$. Solid lines refer to the small-signal model, while dashed lines refer to the exact large-signal solution obtained by simulation. Besides the very good agreement observed with a 10% modulation index, in the case of amplitude modulation (top), we note the well-known split-and-delay effect due to a proper ISOP and a DGD of half a bit before compensation. The intensity distortion then almost disappears after compensation, the residual distortion being due to the residual higher order PMD connected with the eigenmode depolarization, which cannot be compensated for by the previously mentioned first-order OPMDC. The center and bottom figures show instead that the peak-to-peak intensity perturbations induced by common-phase or polarization modulation at the line output are attenuated by the OPMDC, which is a general trend in the many cases, not shown here, that we observed in which the first-order compensator properly works. In addition, the peak-to-peak intensity perturbations caused by the polarization modulation are comparable to those due to the common-mode phase modulation.

We can also try to understand the intensity distortions by reasoning on the frequency behavior of the filters in (4) and (5). Fig. 3 shows $|H_a|$ (top) and both $|H_c|$ and $|H_p|$ (bottom) at the OPMDC input (left column) and output (right column) versus normalized frequency f/R, where $R = 1/T$ is the signal bit rate, for the same line and ISOP values of Fig. 2. Solid lines correspond to the small-signal model, while symbols correspond to the exact values, obtained by simulated transmission through line, or line + OPMDC, of a CW field with $E_i = 1$ and a sinusoidal modulation at frequency f, with a modulation index of 10% of *either* the field amplitude (top row), *or* the common phase, *or* the polarization angle (bottom row). More precisely, open symbols give the ratio of the magnitude of the output intensity spectral line at frequency f to the magnitude of the modulating sinusoid (which we denote as a_M, θ_{c_M}, and θ_{p_M}, respectively, and are all equal to 0.1 in this case). The good agreement between theory and simulations again confirms the validity of (4) with modulation indexes up to 10%. While the shape of $|H_a(\omega)|$ suggests how much an OOK-modulated signal is distorted before and after compensation [9], the shape of $|H_c(\omega)|$ and $|H_p(\omega)|$ tell us that the undesired intensity modulation produced by a neighboring WDM channel through common-phase and polarization modulation contains emphasized frequency components in the high-frequency portion of the signal spectrum, up to $f = R$ and beyond.

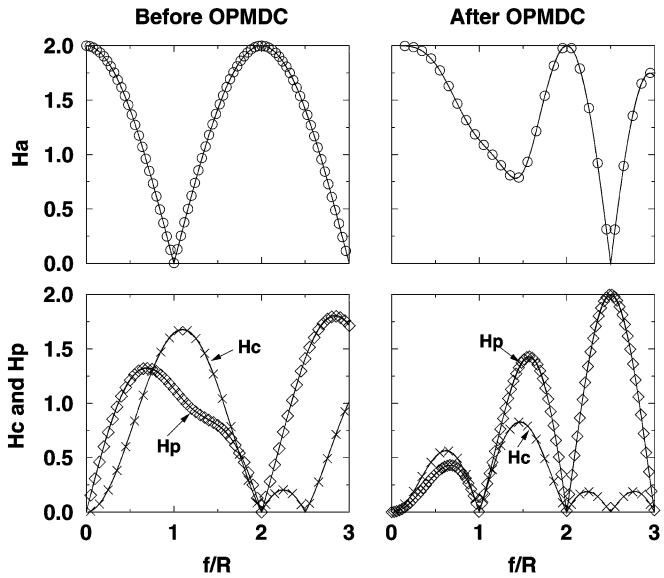

Fig. 3. $|H_a(\omega)|$ (top row) and $|H_c(\omega)|$ and $|H_p(\omega)|$ (bottom row) versus normalized frequency before (left) and after OPMDC (right) for the parameters used in Fig. 2. Solid lines: Small-signal model. Circles, crosses, and diamonds: Simulations for $|H_a(\omega)|$, $|H_c(\omega)|$, and $|H_p(\omega)|$, respectively.

We verified by extensive simulations (not reported here) that, for most line parameters and $\mathbf{J}_i$ values, the polarization modulation has a larger impact on intensity distortion than the common-mode phase modulation, although in special cases the converse may be true, as already mentioned when commenting on (5). As an example, in Fig. 4, we show contour plots of the ratio $\max|H_p|/\max|H_c|$, where $\max|H_p|$ and $\max|H_c|$ are the maximum values of the filters magnitude $|H_c(\omega)|$ and

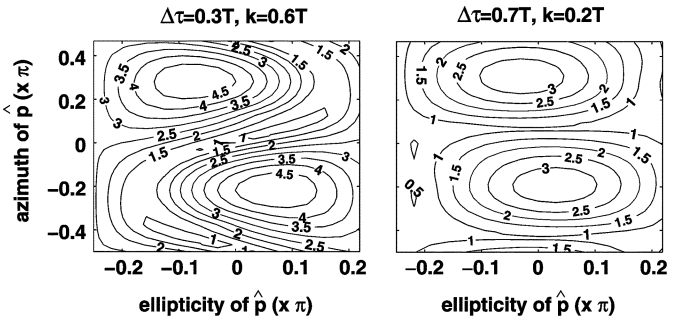

Fig. 4. Contour plot of the ratio $\max|H_p|/\max|H_c|$ versus azimuth and ellipticity of the polarization rotation axis $\hat{p}$ for two different line parameters (reported in each subfigure title) in the case of a line + OPMDC system, and an unperturbed ISOP with azimuth $\theta = \pi/8$ and ellipticity $\varepsilon = \pi/8$.

$|H_p(\omega)|$, respectively, over the band occupied by the main signal lobe $\omega \in [0, 2\pi R]$. The contours are plotted versus the azimuth and the ellipticity of the polarization rotation axis $\hat{p}$ for two different line parameters in the case of a line + OPMDC system and for a generic unperturbed ISOP with azimuth $\theta = \pi/8$ and ellipticity $\varepsilon = \pi/8$, which does not have any specific connection with the symmetry axes of the system. For most orientations of $\hat{p}$, we observe that $\max|H_p| > \max|H_c|$. We also verified that, for the relatively few cases in which $\max|H_p| < \max|H_c|$, the effects of both filters are almost negligible, with $\max|H_c|$ being lower than 0.5. Note that the points of maxima in the contour plots also correspond to the maxima of $\max|H_p|$, which, for the considered ISOP, occur when the rotation axis $\hat{p}$ is close to the Stokes' axes $\pm\hat{s}_2$, that is, when the magnitude of its second component p_2 is maximized (see (5)).

We next analyze in Fig. 5 the effect of line CD and PDL on the intensity filters in the case with OPMDC, where again a good match between model (solid lines) and simulations (symbols) is found for a 10% modulation index.

Fig. 5 (left column) shows $|H_a(\omega)|$ (top) and $|H_c(\omega)|$ and $|H_p(\omega)|$ (bottom) versus normalized frequency when the line used in Fig. 3 now also has a first-order CD corresponding to a line length of 10% of the dispersion length L_D [17].[4] The well-known effect of first-order CD is to introduce oscillations in the intensity filters, which increase the waveform distortions on the input modulating signals, and to emphasize the polarization modulation with respect to the common-phase modulation (see Fig. 3).

Fig. 5 (right column) shows the intensity filters when the system with OPMDC used in Fig. 3 is followed by a diattenuator with PDL = 2 dB and diattenuation axis orthogonal, in Stokes' space, to the unperturbed CW SOP at the output of the OPMDC. Such a situation maximizes the distortion induced by the given PDL. We observe that PDL causes both a common reduction of filter amplitudes and a smoothing of its dips.

Finally, we tested how robust the small-signal model is with respect to modulation index. For the same compensated line as before, we used a 2^7-1 pseudorandom binary sequence (PRBS) of NRZ pulses to modulate the amplitude a, the common phase θ_c, or the polarization angle θ_p.

[4]This is known to produce an ECP of about 0.5 dB in scalar OOK linear systems affected by group-velocity dispersion [18].

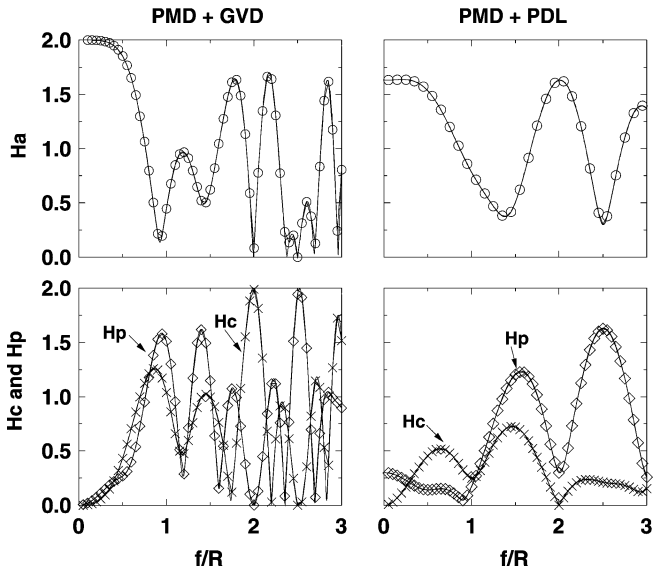

Fig. 5. $|H_a(\omega)|$ (top), $|H_c(\omega)|$, and $|H_p(\omega)|$ (bottom) versus normalized frequency for same system with OPMDC as in Fig. 3, but with added either (left) line group-velocity dispersion corresponding to a dispersion length of 10% of the line length or (right) a 2-dB PDL element at the OPMDC output. Circles, crosses, and diamonds: Simulations for $|H_a(\omega)|$, $|H_c(\omega)|$, and $|H_p(\omega)|$, respectively.

To quantify the linearization error, we evaluated the root-mean-sqaure (rms) deviation

$$d = \sqrt{\frac{\int_0^{T_m} |I_l(t) - I(t)|^2\, dt}{\int_0^{T_m} |I(t)|^2\, dt}}$$

(with T_m being the width of the PRBS window) between the true intensity $I(t)$ and the intensity derived from the small-signal model $I_l(t) = \langle I\rangle|\mathbf{J}|^2 + \Delta I(t)$ obtained by (2).

Fig. 6 shows plots of d versus normalized modulation index for amplitude modulation a, common-phase modulation θ_c, or polarization angle modulation θ_p for (left) the same ISOP with azimuth $\theta = \pi/4$ and ellipticity $\varepsilon = \pi/12$ used in Fig. 2 and (right) a different ISOP with azimuth $\theta = \pi/8$ and ellipticity $\varepsilon = \pi/6$. As a worst case, the Stokes' vector $\hat{p}$ was chosen orthogonal to the ISOP in both situations. We note that the error slightly depends on the ISOP and is larger for the amplitude modulation than for the phase modulations. Since for acceptable curve matching, the rms deviation should stay below roughly $5 \cdot 10^{-2}$ [19], [20], then from the figure, we conclude that the linearized model is reliable for an AM index below about 20%, while a larger index up to about 30% is tolerable for the phase modulations.

What can we conclude from such figures? It is clear that for practical OOK transmission systems, which usually work with extinction ratios in excess of 10 dB, the AM–IM linearized model is not applicable. It could, however, be used to estimate the statistics of accidental intensity modulations induced by small undesired amplitude modulations, such as, for instance, the transmitting laser relative intensity noise, as done in [1].

However, the small-signal model has its most valuable application in the semianalytical BER evaluation procedure that we describe next.

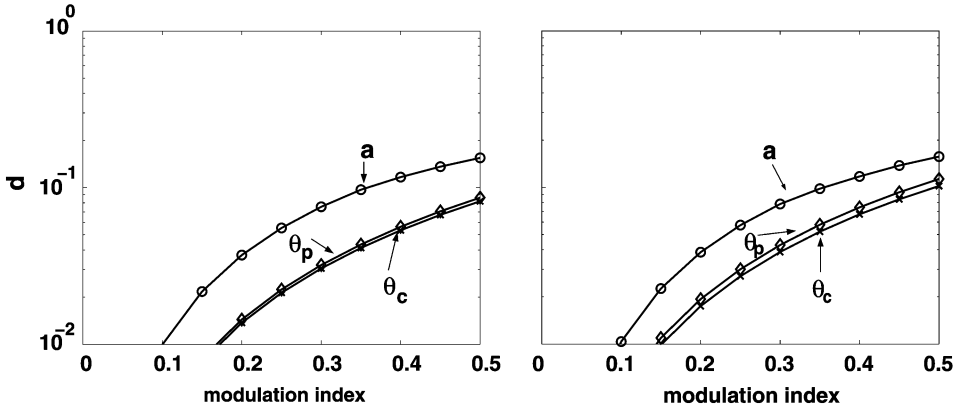

Fig. 6. Root-mean-square (rms) deviation d versus modulation index, computed for the same line of Fig. 3 with OPMDC, for an ISOP (left) with azimuth $\theta = \pi/4$ and ellipticity $\varepsilon = \pi/12$ and (right) with azimuth $\theta = \pi/8$ and ellipticity $\varepsilon = \pi/6$. Solid lines: Small-signal model. Circles, crosses, and diamonds: Simulations with AM–IM, PM–IM, and PolM–IM filters, respectively.

IV. The Semianalytical BER Evaluation Method

The method was originally developed for estimating system penalties in OOK NRZ WDM systems affected by scalar XPM [21]. In this section, we review the main steps and adapt them to the vectorial case at hand.

The key idea is that the interchannel crosstalk due to XPM shows up on the channel of interest as a stochastic additive intensity noise process on mark bits only and is independent of the modulation bits. Therefore, the first step of the method evaluates the received waveform by the beam-propagation method (BPM) [17] when only the channel of interest is transmitted, without amplified spontaneous emission (ASE) noise. This allows construction of the received eye in the absence of crosstalk, accounting for CD and self-phase modulation (SPM) distortions, and the choice of the best sampling time for maximum eye opening. Let $y(t_k)$ be the sampled current at the kth bit time in single-channel noiseless propagation. We assume the preamplified receiver has an optical filter whose bandwidth (which we assume to be five times the bit rate) is large enough not to distort the signal and the XPM-induced crosstalk and only limits the received ASE. An electrical low-pass filter of a bandwidth 0.65 times the bit rate then follows. The total sampled current is then

$$i(t_k) \cong y(t_k) + n(t_k) + x(t_k)$$

where $n(t_k)$ is the electrically low-pass-filtered signal–ASE beat noise, and $x(t_k)$ is the electrically low-pass-filtered XPM-induced crosstalk. The BER$(i(t_k))$ for each kth bit in the PRBS sequence is then found by the total law of probability by conditioning on the sampled crosstalk term

$$\mathrm{BER}(i(t_k)) = \int_{-\infty}^{\infty} \mathrm{BER}(i(t_k) \,|\, x(t_k)) f_x(x)\, dx$$

where $f_x(x)$ is the probability density function (pdf) of the crosstalk term, which we obtain offline by constructing histograms of XPM-induced intensity swings on the probe CW channel. Finally, the total BER is averaged over all bits in the PRBS in order to properly account for intersymbol interference.

Now, the crosstalk pdf can either be estimated by very lengthy BPM simulations or very quickly by using our small-signal filters. Next, we describe how to use the small-signal filters to evaluate the crosstalk statistics. For simplicity, assume there are only two WDM channels, a probe (the channel of interest), and a pump (the channel causing XPM-induced crosstalk on the channel of interest).

The idea is the following. The PMD-impaired fiber is modeled, as usual, as a concatenation of waveplates with randomly oriented PSPs. Within each waveplate, XPM gives a small phase and polarization modulation to the probe [5], [4]. Such a small modulation generated at the waveplate gets converted into an intensity modulation through the PM–IM and PolM–IM filters referred to the equivalent fiber seen from the specific waveplate until the end of the link. Finally, the intensity perturbations generated at all waveplates get added up to yield the received crosstalk intensity. Since all intensity perturbations are obtained from linear filtering of the pump modulation and are added at the output, this amounts to calculating a single compound filter whose input is the pump modulation and whose output is the received crosstalk intensity. Once such a filter is calculated, estimation of the crosstalk pdf is a simple and quick task [21]. Note that in order to calculate the small-signal filters as per (3) and (4), a calculation of the SOP of both pump and probe is needed at the input of each waveplate. To this extent, both channels are supposed to be completely polarized CW, with power equal to their mark power level (recall that we are focusing on the SOP evolution on marks only), whose SOPs are only affected by a frequency-independent rotation, due to the fiber birefringence evaluated at the carrier frequency of each channel. The rotation axis $\hat{p}$ used in filter H_p is computed as the normalized sum of pump and probe ISOPs, according to [4].

The procedure is expected to be accurate—and the linearized PM–IM and PolM–IM filters are expected to hold—when the waveplates are selected short enough that phase and polarization modulations (i.e., the Kerr nonlinearity) in each waveplate are small. The main limit is that the procedure neglects the interaction of SPM and XPM on the probe channel, which is valid when the probe power is not extremely large [21].

As an application of this method, we evaluated the optical signal-to-noise ratio (OSNR) penalty at BER $= 10^{-9}$ for a

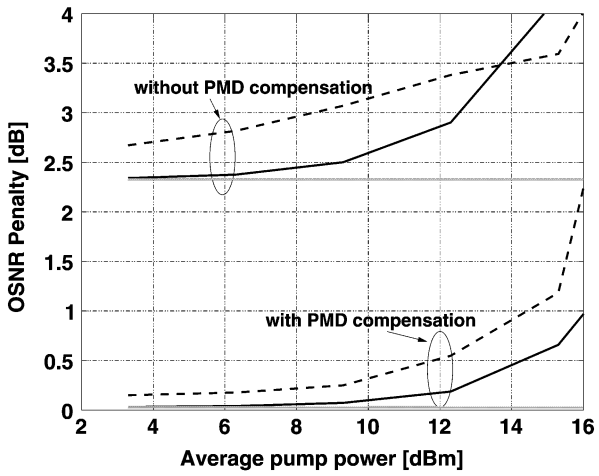

Fig. 7. OSNR penalties (@BER $= 10^{-9}$) of the probe channel ($\bar{P}_s = 3$ dBm) versus $\bar{P}_p$ at the output of a two-channel system with 3×100-km perfectly compensated span of TeraLight fiber and $\Delta\tau = 0.44T$, $k = 0.3T$. Solid lines: Small-signal model. Dashed lines: Simulation. Grey lines: Only PMD.

two-channel system in which the probe and pump signals were spaced by $\Delta\lambda = 0.8$ nm and were OOK modulated by two independent $2^7 - 1$ NRZ PRBS streams at 10 Gb/s. The line consisted of three fully compensated 100-km spans of TeraLight fiber ($D_c = 8$ ps/nm/km, $\gamma = 1.68$ W^{-1}·km^{-1}, and $\alpha = 0.2$ dB/km), where the interaction between PMD and XPM was taken into account through a distributed multisection emulator, as in [4]. At the end of each span, three sections were added before the dispersion-compensating fiber (DCF), and each section emulated a polarization-maintaining fiber with randomly oriented PSPs. The DGD of the whole system was $\Delta\tau = 0.44T$, and the eigenmode rotation rate was $k = 0.3T$, and $\hat{b}(0) = (0.56, -0.52, -0.63)$, that is, almost orthogonal to the input probe SOP. We studied the system both with and without the ideal OPMDC with perfect first-order PMD cancellation that was already used in the previous section. We compared the results given by our small-signal model to the exact numerical results, obtained by applying BPM simulation of the Manakov equation [4]. Because of the BER dependence on the transmitted channels' bit alignment, the simulated results were averaged over 20 different time delays between pump and probe bits. With the small-signal model, instead, the crosstalk pdf averaged over all possible delays is directly obtained.

In Fig. 7, we show the OSNR penalty obtained both with numerical simulations (dashed line) and with our small-signal model (solid line) for a probe ISOP $\hat{j}$ with $\theta = \pi/12$ and $\epsilon = \pi/8$ and a pump ISOP aligned with $\hat{s}_3$, that is, for a relative polarization angle of $\pi/4$ between pump and probe ISOPs [4]. The average power of the probe was fixed at 3 dBm, while the pump average power $\bar{P}_p$ was varied from 3.3 to 16 dBm. In all cases, the received OSNR of the probe channel was 21 dB/0.1 nm. The constant grey lines describe the OSNR penalty measured with only PMD, both with and without OPMDC. With only XPM, we measured a negligible OSNR penalty of 0.5 dB in the worst case $\bar{P}_p = 16$ dBm. The efficiency of PMD compensation starts to be significantly affected by the interplay between XPM and PMD when $\bar{P}_p > 15$ dBm, where an additional penalty larger than 1 dB is found. Roughly, this corresponds to the compound effect of 16 neighboring WDM channels if the walkoff effect is ignored, and many more when CD-induced walkoff is taken into account. We note that the system without OPMDC suffers a much larger penalty, exceeding 1 dB beyond $\bar{P}_p = 12$ dBm. In both cases with and without OPMDC, the analytical results show a maximum difference from the numerical results of about 0.5 dB. However, the analytical model is not able to fit the simulated curves when the large strength of XPM nonlinear effects rapidly degrades the system performance, that is, beyond a threshold power of 14 dBm for the noncompensated system and of 15 dBm for the compensated one. Note that an OPMDC with a degree of polarization (DOP) as feedback control, which works without tracking the fiber PSPs, is expected to give worse performance than that shown in Fig. 7, because its best operating conditions could be hidden by the depolarizing effects on DOP due to interaction of PMD and XPM [4].

V. Conclusion

This paper presented a vectorial generalization of the small-signal scalar model of Wang and Petermann [1] for evaluation of the received intensity out of general optical transmission systems affected by CD, PMD, and PDL in the presence of amplitude, phase, and polarization modulations with small modulation indexes. The novel formulation shows that the intensity modulation in all cases can be obtained as a linear-weighted combination of the components of the Stokes' vector of the unperturbed ISOP. Such a result, which also holds for the large-signal IM–IM transfer function, allows, for instance, a simple search of the best/worst ISOPs for each modulation format.

As an application, we have checked the amplitude, phase, and polarization modulation conversion in transmission lines with and without first-order OPMDC. We have verified that there exists a whole set of ISOPs—those on the plane, including the line eigenmode and its rotation axis—for which the PM–IM conversion is minimal, while for the two ISOPs orthogonal to such a plane, both the AM–IM conversion is minimal (largest AM distortion on desired OOK signal) and the PM–IM (undesired) conversion is largest. In addition, for most lines and ISOPs, the polarization modulation is found to give a larger intensity modulation than common-mode phase modulation. It was found that first-order compensation, when properly working (i.e., with nondominant higher order PMD effects, such as eigenmodes depolarization), also has the ability to reduce the peak-to-peak intensity excursions due to both common PM and PolM. It has been verified that the linearized model provides excellent predictions of the output intensity when the modulation index is below 10% and acceptable predictions up to modulation indexes of about 20% for the AM and of about 30% for PM and PolM.

Finally, a semianalytical BER evaluation method that was originally developed for the scalar XPM case was adapted to the case of vectorial XPM. It was shown in a simple case study that the method is able to quantify the system penalty induced by the interplay of XPM, CD, and PMD in dispersion-mapped WDM systems.

APPENDIX A

It is proven in this Appendix that the frequency responses in (3) can be cast in the form (4).

Starting from $V(\omega) = \underline{v}(\omega)\cdot\underline{\sigma}$, it is noted that, since the Pauli matrices are Hermitian, then $V^{\dagger}(-\omega) = (\sum_i v_i(-\omega)\sigma_i)^{\dagger} = \underline{v}^*(-\omega)\cdot\underline{\sigma}$. Hence, substitution in the first two relations in (3) gives the equation shown at the bottom of the page, where we used the linearity property [13, eq. (A.13)]. Such equations immediately give the first two relations in (4). To prove the third relation, we first prove that

$$\underline{l} \triangleq \mathbf{J}_i^{\dagger}\underline{\sigma}\mathbf{L} = P\underline{j}$$

where $\mathbf{L} \triangleq (\hat{p}\cdot\vec{\sigma})\mathbf{J}_i$ and P is the 4×4 matrix defined in block form in Section II. Write such a 4×1 vector in block partitioned form as $\underline{l} = [l_0; \vec{l}]$, where l_0 is its first component and $\vec{l}$ the 3×1 vector of its remaining components. Using [13, eq. (A.3)], we first write $\vec{\sigma}(\hat{p}\cdot\vec{\sigma}) = \sigma_0\hat{p} - i\vec{\sigma}\times\hat{p}$. Then, using [13, eq. (A.13)], we have $\vec{l} = \mathbf{J}_i^{\dagger}\vec{\sigma}(\hat{p}\cdot\vec{\sigma})\mathbf{J}_i = (\mathbf{J}_i^{\dagger}\sigma_0\mathbf{J}_i)\hat{p} - i(\mathbf{J}_i^{\dagger}\vec{\sigma}\mathbf{J}_i)\times\hat{p} = \hat{p} - i\hat{j}\times\hat{p}$. Similarly, we find: $l_0 = \mathbf{J}_i^{\dagger}(\hat{p}\cdot\vec{\sigma})\mathbf{J}_i = \hat{p}\cdot\hat{j}$.

Hence, in block form, $\underline{l} = [\hat{p}\cdot\hat{j}; \hat{p} - i\hat{j}\times\hat{p}] = P\underline{j}$.

Thus, again using the linearity property [13, eq. (A.13)], the third relation in (3) writes as

$$\begin{aligned} H_p(\omega) &= \frac{1}{i}[\mathbf{J}_i^{\dagger}\underline{v}(\omega)\cdot\underline{\sigma}\mathbf{L} - \mathbf{L}^{\dagger}\underline{v}^*(-\omega)\cdot\underline{\sigma}\mathbf{J}_i] \\ &= \frac{1}{i}[\underline{v}(\omega)\cdot(\mathbf{J}_i^{\dagger}\underline{\sigma}\mathbf{L}) - \underline{v}^*(-\omega)\cdot(\mathbf{L}^{\dagger}\underline{\sigma}\mathbf{J}_i)] \\ &= \frac{1}{i}[\underline{v}(\omega)\cdot P\underline{j} - \underline{v}^*(-\omega)\cdot P^*\underline{j}] \\ &= \frac{1}{i}[\underline{v}^T(\omega)P - \underline{v}^{\dagger}(-\omega)P^*]\underline{j}. \end{aligned}$$

From the block form of P in Section II, we note that $P^* = P^T$, since $(i\hat{p}\times)^T = -i\hat{p}\times$. Thus, $P^{T^*} = P$, that is, P is Hermitian. Hence

$$\begin{aligned} H_p(\omega) &= \frac{1}{i}[\underline{v}^T(\omega)P - \underline{v}^{\dagger}(-\omega)P^T]\underline{j} \\ &= \frac{1}{i}[P^T\underline{v}(\omega) - P\underline{v}^*(-\omega)]\cdot\underline{j} \end{aligned}$$

which proves the third relation in (4).

APPENDIX B

In this Appendix, the line + OPMDC system is analyzed. The compensator is composed of a tunable polarization controller (PC), followed by a polarization-maintaining fiber (PMF). It is assumed that the PC can orient the PMF eigenmode in any position on the Poincaré sphere. The Jones matrix $U_C(\omega)$ of the PC + PMF compensator as [10] is modeled as

$$\begin{aligned} &U_C(\omega) = U_{C0}V_C(\omega) \\ &V_C(\omega) \triangleq \cos\left(\frac{\Delta\phi_c(\omega)}{2}\right)\sigma_0 - i\sin\left(\frac{\Delta\phi_c(\omega)}{2}\right)(\hat{c}\cdot\vec{\sigma}) \end{aligned} \tag{6}$$

where U_{C0} is the compensator matrix at the reference frequency, $\Delta\phi_c(\omega)$ is its retardation angle, and $\hat{c}$ is the unit eigenmode of the extracted compensator matrix $V_C(\omega)$.

The line fiber is described by the unitary Jones matrix

$$\begin{aligned} &U_F(\omega) = V_L(\omega)U_{F0} \\ &V_L(\omega) \triangleq \cos\left(\frac{\Delta\phi_l(\omega)}{2}\right)\sigma_0 - i\sin\left(\frac{\Delta\phi_l(\omega)}{2}\right)(\hat{b}(\omega)\cdot\vec{\sigma}) \end{aligned}$$

where $\Delta\phi_l(\omega)$ and $\hat{b}(\omega)$ are its retardation angle and eigenmode, respectively.

The Jones matrix of the total system composed of line + OPMDC is

$$T(\omega) = U_C(\omega)U_F(\omega) = U_{C0}W(\omega)U_{F0} \tag{7}$$

where $W(\omega) \triangleq V_C(\omega)V_L(\omega)$ contains all the frequency dependence of the global Jones matrix, and $W(0)$ equals the identity matrix. Now evaluation of the matrix $V(\omega)$ in (3) gives

$$V(\omega) = T^{\dagger}(0)T(\omega) = U_{F0}^{\dagger}W(\omega)U_{F0}.$$

If one uses such a matrix in (3) and one goes through the derivation steps in Appendix A, one realizes that the result (4) also holds if one uses the Pauli coordinates $\underline{w}$ of $W(\omega)$ instead of the Pauli coordinates $\underline{v}$ of $V(\omega)$ and if both the ISOP $\hat{j}$ and the polarization rotation axis $\hat{p}$ are expressed in the coordinate system rotated by the Mueller matrix associated with the unitary Jones matrix U_{F0}.

In order to get explicit expressions of the filters in (4), it is now necessary to derive the Pauli vector $\underline{w}$ of $W(\omega)$.

Since the Pauli vector of the compensator V_C is $\underline{v}_c(\omega) = [\cos(\Delta\phi_c(\omega)/2); -i\sin(\Delta\phi_c(\omega)/2)\hat{c}]$ and that of the line V_L is $\underline{v}_l(\omega) = [\cos(\Delta\phi_l(\omega)/2); -i\sin(\Delta\phi_l(\omega)/2)\hat{b}(\omega)]$, by the concatenation rule for Pauli vectors ([10, eq. (A.3)], the Pauli vector of the total Jones matrix $W(\omega)$ is obtained as

$$\underline{w} = \begin{bmatrix} \delta(\omega) - \beta(\omega)(\hat{c}\cdot\hat{b}(\omega)) \\ -i\{\gamma(\omega)\hat{b}(\omega) + \alpha(\omega)\hat{c} + \beta(\omega)(\hat{c}\times\hat{b}(\omega))\} \end{bmatrix} \tag{8}$$

$$\begin{cases} H_a(\omega) = \mathbf{J}_i^{\dagger}[\underline{v}(\omega)\cdot\underline{\sigma} + \underline{v}^*(-\omega)\cdot\underline{\sigma}]\mathbf{J}_i = (\underline{v}(\omega) + \underline{v}^*(-\omega))(\mathbf{J}_i^{\dagger}\underline{\sigma}\mathbf{J}_i) \\ H_c(\omega) = \frac{\mathbf{J}_i^{\dagger}}{i}[\underline{v}(\omega)\cdot\underline{\sigma} - \underline{v}^*(-\omega)\cdot\underline{\sigma}]\mathbf{J}_i = \frac{\underline{v}(\omega) - \underline{v}^*(-\omega)}{i}(\mathbf{J}_i^{\dagger}\underline{\sigma}\mathbf{J}_i) \end{cases}$$

where

$$\begin{cases} \alpha \triangleq \sin\left(\frac{\Delta\phi_c}{2}\right)\cos\left(\frac{\Delta\phi_l}{2}\right) \\ \beta \triangleq \sin\left(\frac{\Delta\phi_c}{2}\right)\sin\left(\frac{\Delta\phi_l}{2}\right) \\ \gamma \triangleq \cos\left(\frac{\Delta\phi_c}{2}\right)\sin\left(\frac{\Delta\phi_l}{2}\right) \\ \delta \triangleq \cos\left(\frac{\Delta\phi_c}{2}\right)\cos\left(\frac{\Delta\phi_l}{2}\right). \end{cases} \tag{9}$$

It can be shown that the concatenation rule (8) has a simple geometrical interpretation on the Poincaré sphere [10]. This fact is of great importance, since it provides the eigenmodes description with a graphical tool much similar to the graphical interpretation of the concatenation rule for the PMD vector and can be effectively used to visualize the action of OPMDCs [22], although this point will not be expanded on in the present paper.

In the specific example, $\Delta\phi_c = \Delta\phi_l = \Delta\tau\omega$, $\hat{b}(0) = \hat{s}_1$, and $\hat{c} = -\hat{b}(0)$ are selected. Moreover, according to the choice of the rotation model around $\hat{k} = \hat{s}_3$, the eigenmode equation is $\hat{b}(\omega) = \cos(k\omega)\hat{s}_1 + \sin(k\omega)\hat{s}_2$. Substitution in (8) yields the desired Pauli vector

$$\begin{aligned} \underline{w}(\omega) = \Bigg[& \cos^2\left(\frac{\Delta\tau\omega}{2}\right) + \sin^2\left(\frac{\Delta\tau\omega}{2}\right)\cos(k\omega); \\ & i\sin(\Delta\tau\omega)\sin^2\left(\frac{k\omega}{2}\right); -\frac{i}{2}\sin(\Delta\tau\omega)\sin(k\omega); \\ & i\sin^2\left(\frac{\Delta\tau\omega}{2}\right)\sin(k\omega)\Bigg]. \end{aligned} \tag{10}$$

ACKNOWLEDGMENT

The authors would like to thank E. Corbel, S. Lanne, and S. Bigo for stimulating interactions.

REFERENCES

[1] J. Wang and K. Petermann, "Small-signal analysis for dispersive optical fiber communication systems," *J. Lightw. Technol.*, vol. 10, no. 1, pp. 96–100, Jan. 1992.

[2] R. Khosravani, Y. Xie, L.-S. Yan, Y. W. Song, A. E. Willner, and C. R. Menyuk, "Limitations to first-order PMD compensation in WDM systems due to XPM-induced PSP changes," in *Proc. Optical Fiber Communication Conf. (OFC 2001)*, vol. 3, 2001, pp. WAA5.1–WAA5.3.

[3] J. H. Lee, K. J. Park, C. H. Kim, and Y. C. Chung, "Effects of nonlinear crosstalk in optical PMD compensation," *IEEE Photon. Technol. Lett.*, vol. 14, no. 8, pp. 1082–1084, Aug. 2002.

[4] A. Bononi, A. Vannucci, A. Orlandini, E. Corbel, S. Lanne, and S. Bigo, "Degree of polarization degradation due to cross-phase modulation and its impact on polarization mode dispersion compensators," *J. Lightw. Technol.*, vol. 21, no. 9, pp. 1903–1913, Sep. 2003.

[5] B. C. Collings and L. Boivin, "Nonlinear polarization evolution induced by cross-phase modulation and its impact on transmission systems," *IEEE Photon. Technol. Lett.*, vol. 12, no. 11, pp. 1582–1584, Nov. 2000.

[6] G. Bellotti, M. Varani, C. Francia, and A. Bononi, "Intensity distortion induced by cross-phase modulation and chromatic dispersion in optical-fiber transmissions with dispersion compensation," *IEEE Photon. Technol. Lett.*, vol. 10, no. 12, pp. 1745–1747, Dec. 1998.

[7] A. V. T. Cartaxo, "Cross-phase modulation in intensity modulation-direct detection WDM systems with multiple optical amplifiers and dispersion compensators," *J. Lightw. Technol.*, vol. 17, no. 2, pp. 178–190, Feb. 1999.

[8] R. I. Killey, H. J. Thiele, V. Mikhailov, and P. Bayvel, "Prediction of transmission penalties due to cross-phase modulation in WDM systems using a simplified technique," *IEEE Photon. Technol. Lett.*, vol. 12, no. 7, pp. 804–806, Jul. 2000.

[9] R. Noé, D. Sandel, M. Y. Dierolf, S. Honz, V. Mirvoda, A. Schoplin, C. Glingener, E. Gottwald, C. Scheerer, G. Fisher, T. Weyerauch, and W. Haase, "Polarization mode dispersion compensation at 10, 20, and 40 Gbit/s with various optical equalizers," *J. Lightw. Technol.*, vol. 17, no. 9, pp. 1602–1615, Sep. 1999.

[10] A. Bononi and A. Vannucci, "Is there life beyond the principal states of polarization?," *Optical Fiber Technol.*, vol. 8, pp. 257–294, 2002.

[11] A. Eyal, D. Kuperman, and M. Tur, "An efficient technique for finding input SOP's, which maximize/minimize the eye-opening in fiber-optic links with high-order PMD and PDL," presented at the Optical Fiber Communication Conf. (OFC 2003), Atlanta, GA, Mar. 2003. Paper ThJ5.

[12] R. Noé, D. Sandel, V. Mirvoda, F. Wüst, and S. Hinz, "Polarization mode dispersion detected by arrival time measurement of polarization-scrambled light," *J. Lightw. Technol.*, vol. 20, no. 2, pp. 229–235, Feb. 2002.

[13] J. P. Gordon and H. Kogelnik, "PMD fundamentals: Polarization mode dispersion in optical fibers," in *Proc. Nat. Academy Science (PNAS)*, vol. 97, Apr. 2000, pp. 4541–4550.

[14] N. J. Frigo, "A generalized geometrical representation of coupled mode theory," *IEEE J. Quantum Electron.*, vol. QE-22, no. 11, pp. 2131–2140, Nov. 1986.

[15] H. Kogelnik, L. E. Nelson, and J. P. Gordon, "Emulation and inversion of polarization-mode dispersion," *J. Lightw. Technol.*, vol. 21, no. 2, pp. 482–495, Feb. 2003.

[16] F. Bruyere, "Impact of first- and second-order PMD in optical digital transmission systems," *Optical Fiber Technol.*, vol. 2, pp. 269–280, 1996.

[17] G. P. Agrawal, *Nonlinear Fiber Optics*. San Diego, CA: Academic, 1989.

[18] A. F. Elrefaie, R. E. Wagner, D. A. Atlas, and D. G. Daut, "Chromatic dispersion limitations in coherent lightwave transmission systems," *J. Lightw. Technol.*, vol. 6, no. 5, pp. 704–709, May 1988.

[19] A. Vannucci, P. Serena, and A. Bononi, "The RP method: A new tool for the iterative solution of the nonlinear Schroedinger equation," *J. Lightw. Technol.*, vol. 20, no. 7, pp. 1102–1112, Jul. 2002.

[20] O. V. Sinkin, R. Holzlöhner, J. Zweck, and C. R. Menyuk, "Optimization of the split-step Fourier method in modeling optical-fiber communications systems," *J. Lightw. Technol.*, vol. 21, no. 1, pp. 61–68, Jan. 2003.

[21] G. Bellotti, "A survey of dispersion maps for 10 Gb/s terrestrial transmissions, with network applications," in *Optical Networking*, A. Bononi, Ed. London, U.K.: Springer-Verlag, 1999, pp. 212–221.

[22] A. Vannucci, A. Bononi, and L. Gavini, "A new control for double-stage optical PMD compensators and its geometrical interpretation," presented at the Eur. Conf. Optical Communication (ECOC 2003), Rimini, Italy, Sep. 2003. Paper We.3.6.3.

Alberto Bononi, photograph and biography not available at the time of publication.

Alessandra Orlandini (S'00–M'01), photograph and biography not available at the time of publication.